



HAL
open science

Fabrication and characterization of tapered photonic crystal fiber for broadband $2 \mu\text{m}$: four-wave mixing-based fibered OPCPA

Sidi-Ely Ahmedou, Guillaume Walter, Jules Herbuvaux, Romain Dauliat, Sébastien Février, Stéphane Petit, Constance Valentin, Denis Marion, Jérôme Lhermite, Laurent Labonté, et al.

► To cite this version:

Sidi-Ely Ahmedou, Guillaume Walter, Jules Herbuvaux, Romain Dauliat, Sébastien Février, et al.. Fabrication and characterization of tapered photonic crystal fiber for broadband $2 \mu\text{m}$: four-wave mixing-based fibered OPCPA. Applied Physics B - Laser and Optics, 2023, 129, 10.1007/s00340-023-08012-z . hal-04074716

HAL Id: hal-04074716

<https://hal.science/hal-04074716>

Submitted on 19 Apr 2023

HAL is a multi-disciplinary open access archive for the deposit and dissemination of scientific research documents, whether they are published or not. The documents may come from teaching and research institutions in France or abroad, or from public or private research centers.

L'archive ouverte pluridisciplinaire **HAL**, est destinée au dépôt et à la diffusion de documents scientifiques de niveau recherche, publiés ou non, émanant des établissements d'enseignement et de recherche français ou étrangers, des laboratoires publics ou privés.



Fabrication and characterization of tapered photonic crystal fiber for broadband 2 μm : four-wave mixing-based fibered OPCPA

Sidi-Ely Ahmedou¹ · Guillaume Walter² · Jules Herbuvaux² · Romain Dauliat¹ · Sébastien Février¹ · Stéphane Petit² · Constance Valentin² · Denis Marion² · Jérôme Lhermite² · Laurent Labonté³ · Sébastien Tanzilli³ · Frédéric Gérôme¹ · Benoit Debord¹ · Fetah Benabid¹ · Baptiste Leconte¹ · Guy Millot^{4,5} · Phillipe Roy¹ · Raphaël Jamier¹ · Jean-Christophe Delagnes²

Received: 29 November 2022 / Accepted: 27 March 2023
© The Author(s) 2023

Abstract

We present the simulation, fabrication, and characterization of large area microstructured fiber tapers which enables broadband phasematching conditions of the four wave-mixing process. These silica-based tapers are intended to serve as a nonlinear gain medium for intense and high average power Fiber Optical Parametric Chirped Pulse Amplifier emitting at 2 μm and strongly pumped at Yb wavelength. Different geometries (tapered/untapered, aspect ratio, etc.) are fabricated, analyzed and their broadening properties—key for supporting ultrashort pulses amplification—are compared and discussed. The characterization of nonlinear gain bandwidth of the tapers relies on a tunable source of stochastic pulses based on tunable amplified spontaneous emission in Yb-doped amplifiers. The strong overshoots of this source allows degenerate four-wave mixing process to occur thus generating broadband incoherent visible signal and mid-infrared idler waves at much lower average power than usually needed with coherent pumping. The idler centered around 1.85 μm is broadened due to zero-dispersion wavelength shift along the taper.

Keywords Photonic crystal fiber · Four wave mixing · Middle infrared · Amplified spontaneous emission

1 Introduction

Myriads of middle-infrared (midIR, 1400–3000 nm) applications require either broadband ultra-short pulses or wide tunability. In recent years, lots of research have been conducted on solid-state laser materials emitting in the midIR spectral

range (such as Tm³⁺, Ho³⁺, Cr²⁺ or/and Er³⁺-doped materials) [1, 2]. However, these active materials cannot directly generate few-cycles pulses (FCP) without a nonlinear (post-compression) stage [3, 4].

Optical parametric (chirped pulses) amplifiers (OP(CP)A) using second-order nonlinear processes are often used as an alternative approach. Bulk or structured nonlinear crystals, such as BBO, KTA, or APPLN (Aperiodically Poled Lithium Niobate), have successfully been used to produce broadly tunable coherent midIR radiations [5] or wide spectra compatible with FCP with a passive stabilization of the carrier-to-envelope phase (CEP) [6]. While they exhibit a very good efficiency and exceptionally high damage threshold and/or low thermal loads at high repetition rate, crystal-based OP(CP)A generally suffers from rather poor beam quality. Thus, more recently, fibered OPCPA (f-OPCPA) based on third-order four-wave mixing (FWM) process have been proposed, to exploit the advantages of fiber confinement [7]. This confinement can be in the form of a hollow-core fiber with a FWM in gas [8], or in

✉ Raphaël Jamier
raphael.jamier@xlim.fr

✉ Jean-Christophe Delagnes
jean-christophe.delagnes@u-bordeaux.fr

¹ XLIM, Université de Limoges, CNRS, UMR 7252, 123, av. Albert Thomas, 87060 Limoges, France

² CELIA, Université de Bordeaux, CNRS, CEA, UMR 5107, 43, rue Pierre Noailles, 34000 Talence, France

³ INPHYNI, Université Côte d'Azur, CNRS, UMR 7010, av. Joseph Vallot, 06108 Nice, France

⁴ ICB, Université de Bourgogne, CNRS, UMR 6303, 9, av. Alain Savary, 21078 Dijon, France

⁵ Institut Universitaire de France (IUF), 1, rue Descartes, Paris, France

dispersion-engineered fibers, where its use near the zero-dispersion wavelength generated a broadband spectrum [9].

In this paper, we explore the generation of a broadband spectrum in the midIR through degenerated Four-Wave Mixing (d-FWM) far from the zero-dispersion wavelength (ZDW). This process, occurring in centrosymmetric media such as silica, is characterized by the generation of a pair of photons (resp. signal λ_s and idler λ_i with $\lambda_s < \lambda_i$), from two pump photons at λ_p .

In order to characterize the taper properties, the gain bandwidth and phase matching curves are usually retrieved by measuring (as a function of the pump wavelength and power) the signal and the idler spectra resulting from the parametric generation (i.e unseeded or spontaneous). This technique has been widely applied for characterizing uniform fibers or fibers with exotic shapes and materials [10], or else directly for FWM-based Optical Parametric Oscillators (OPO) and Amplifiers (OPA) [11–14].

Through the phase matching curve of d-FWM process, large tuning ranges are accessible by tuning the central pump wavelength [15]. However at a fixed pump wavelength, the gain bandwidths obtained are relatively narrow. Highly nonlinear photonic crystal fibers (HNL-PCF) exhibit numerous advantages for spectrum broadening, with their large flexibility in design and the related chromatic dispersion management.

Our aim is to investigate home-made tapered HNL-PCF (later referred as "taper") which ZDW and higher-order dispersion shift along the taper in order to extend the range of d-FWM parametric gain over a spectral width of typically 200 nm at 1.8 μm . As shown later, this is 4 times larger than the spectrum obtained with the same untapered HNL-PCF.

2 Fabrication of taper

The fabrication of long tapers suited for parametric amplification raises several challenges. First the taper profile must vary smoothly enough (adiabatic variation) in order to preserve the transmission properties, to prevent random perturbation in the profile, to provide the required phasematching properties. Secondly one must avoid any hole coalescence. As a consequence, we have developed the following fabrication procedure.

A constant diameter PCF is initially fabricated using the conventional "stack and draw" method. In such fibers the transverse profile geometry is characterized by the core diameter d_{core} , the air-holes diameter d_{hole} and the pitch Λ (distance between two adjacent air-holes). This fiber can serve as a reference to compare the effect of spectral broadening investigated later.

The tapers are then obtained by reducing the PCF size. In practice, during the fabrication of the tapered fiber, the key

Table 1 Tapers characteristics: $\phi_{\text{clad},<}$ and $\phi_{\text{clad},>}$ are the smallest and the largest external diameters, L is the taper length. Fiber A external diameter is constant

Taper name	$\phi_{\text{clad},<} (\mu\text{m})$	$\phi_{\text{clad},>} (\mu\text{m})$	L (m)
A	128	128	2
B	125	132	2
C	125	128	1.2
D ₁	132	139	1.3
D ₂	132	139	2

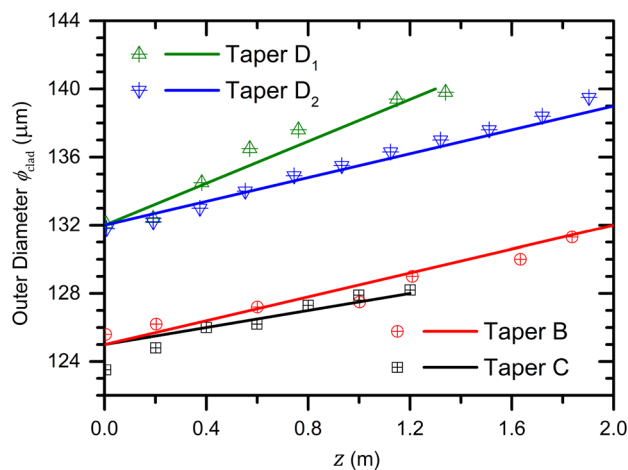


Fig. 1 Variation of the measured external diameter for the taper B, C, D₁, and D₂

parameter is the outer (cladding) diameter ϕ_{clad} , however, the other geometrical parameters (core and air holes sizes) of the structure vary in a homothetic way (e.g. $\phi_{\text{clad}} = 125 \mu\text{m}$ and $d_{\text{core}} = 6.49 \mu\text{m}$ for $\Lambda_0 = 4.5 \mu\text{m}$ while $\phi_{\text{clad}} = 139 \mu\text{m}$ and $d_{\text{core}} = 7.20 \mu\text{m}$ for $\Lambda_0 = 5.0 \mu\text{m}$). Note that the homothety assumption is valid for the relative size variations $<5\%$ targeted here (see Table 1).

The size reduction is controlled by varying the coiling speed using a home-made automated software. Indeed at a fixed temperature and gas pressure, and assuming a homothety between the outer fiber diameter and all the other quantities, we can see from the mass flow conservation law between the preform (diameter ϕ_p , speed v_p) and the fiber (diameter ϕ_{clad} , speed v_f):

$$\phi_p^2 \times v_p = \phi_{\text{clad}}^2 \times v_f \quad (1)$$

that the fiber diameter ϕ_{clad} can be controlled by adjusting the drawing speed v_f . An in-line measurement monitors the outer diameter during the taper drawing (Fig. 1).

In order to explore the influence of the taper slope, length, and smallest/largest diameter, four different tapers

respectively denoted B, C, D₁ and D₂ along with a reference fiber A were drawn and further characterized.

3 Numerical simulations

The proposed tapered HNL-PCF is based on a small and continuous variation applied on the external diameter of the fiber. The idea is to longitudinally change the dispersion properties of the fiber experienced by the pump radiation (close to 1.03 μm) and particularly its "local" zero-dispersion wavelength (ZDW) which progressively shift along the propagation. The concept is similar to an APPLN crystal, where the linear aperiodicity shifts the generated signal along the crystal [16]. As a consequence both the generated signal and idler output spectra are broadened. Compared to a uniform diameter fiber of the same length, a given d-FWM bandwidth within this composite spectrum is generated over a shorter fiber segment, thus reducing its parametric gain. In order to maintain a high parametric gain, the taper needs to be lengthened. Moreover, as the core diameter decreases, the effective nonlinear coefficient γ varies inversely:

$$\gamma = n_2\omega/A_{\text{eff}}c \tag{2}$$

with n_2 the nonlinear refractive index change due to Kerr effect, and A_{eff} the effective mode area. The interplay between these effects results in a complex behaviour than can be rendered by numerical simulations based on the general nonlinear Schrödinger equation (GNLSE) [17]. Nonetheless, accurately modelling the GNLSE including the minute details of the taper variation, although feasible, brings no further insight into the overall spectrum features, and we

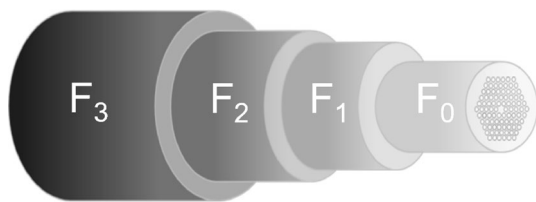


Fig. 2 Schematic representation of the tapered HNL-PCF used in simulations: the taper is divided into $N = 4$ fiber segments (F_0, F_1, F_2, F_3), whose characteristic size varies linear from F_0 to F_3

thus modelled the taper by dividing it into four different segments each being uniform as represented in Fig. 2.

The four fiber segments (noted F_0, F_1, F_2 and F_3 all 30 cm long) possess different external diameters, as shown in Fig. 2. The geometrical properties of the i -th segment are incremented according to $\Lambda_i = \Lambda_0 \times (1 + i \times 1.5\%)$, with $\Lambda_0 = 4.5 \mu\text{m}$ and the ratio $d_{\text{hole},i}/\Lambda_i = 0.59$ is kept constant. As an example, for each i -th section of the taper considered in our simulation, the outer diameter and ZDW are reported in Table 2.

The change in geometric parameters (core diameter, pitch, air-hole diameter) due to outer diameter variations causes the dispersion properties to vary. The most important parameter being the ZDW that is gradually shifting (see Table 2). The higher-order dispersion terms $\beta_{n,\text{ZD}}$ are also varying along the taper (see Table 3). They too play an important role along the ZDW since the Stokes shift $\Omega(\omega_{s,i} = \omega_p \pm \Omega)$ with respect to the pump angular frequency ω_p is given by:

$$\Omega(\omega_p) = \left(- \left(Q + \sqrt{Q^2 - 4P\beta_{\text{NL}}} \right) / 2P \right)^{1/2} \tag{3}$$

where $P = (\beta_{4,\text{ZD}} + \beta_{5,\text{ZD}} \cdot (\omega_p - \omega_{\text{ZD}})) / 12$ and $Q = \beta_{3,\text{ZD}} \cdot (\omega_p - \omega_{\text{ZD}}) + \beta_{4,\text{ZD}} \cdot (\omega_p - \omega_{\text{ZD}})^2 / 2 + \beta_{5,\text{ZD}} \cdot (\omega_p - \omega_{\text{ZD}})^3 / 6$ with ω_{ZD} the zero-dispersion angular frequency, β_{NL} the nonlinear dispersion due to the cross-Kerr effect induced by the pump, and the $\beta_{n,\text{ZD}}$ are the n -th-order dispersion evaluated at ω_{ZD} . As a consequence, the d-FWM phasematching curve is gradually changing along the taper as ω_{ZD} , the $\beta_{n,\text{ZD}}$, and β_{NL} vary with the taper cross-section thus leading to a broadened gain spectrum.

Moreover, as illustrated in Fig. 3a, the group index n_g varies by ~ 0.01 between the signal and idler wavelengths. This group velocity mismatch (GVM) may reduce the temporal overlap between the pump, the signal to be amplified and the resulting idler. However, this is not the case for the ASE source used here since its 50 ps are long enough to overcome this effect. However, as far as f-OPCPA is concerned,

Table 3 High-order propagation constant $\beta_{n,\text{ZD}}$ for $n = 3, 4,$ and 5 evaluated at the ZDW for 125, 128, 132, and 139 μm outer diameters

$\phi_{\text{clad}} (\mu\text{m})$	125	128	132	139
$\beta_{3,\text{ZD}} (\times 10^{-3} \text{ ps}^3/\text{km})$	63.3	63.4	63.6	63.9
$\beta_{4,\text{ZD}} (\times 10^{-4} \text{ ps}^4/\text{km})$	- 1.14	- 1.15	- 1.16	- 1.18
$\beta_{5,\text{ZD}} (\times 10^{-7} \text{ ps}^5/\text{km})$	3.39	3.45	3.55	3.64

Table 2 Outer diameter ϕ_{clad} and ZDW (in μm) of the F_0, F_1, F_2 and F_3 sections used in the simulation of the taper in Fig. 2

F_0		F_1		F_2		F_3	
ϕ_{clad}	ZDW	ϕ_{clad}	ZDW	ϕ_{clad}	ZDW	ϕ_{clad}	ZDW
125	1.068	127.33	1.071	129.66	1.075	132	1.080

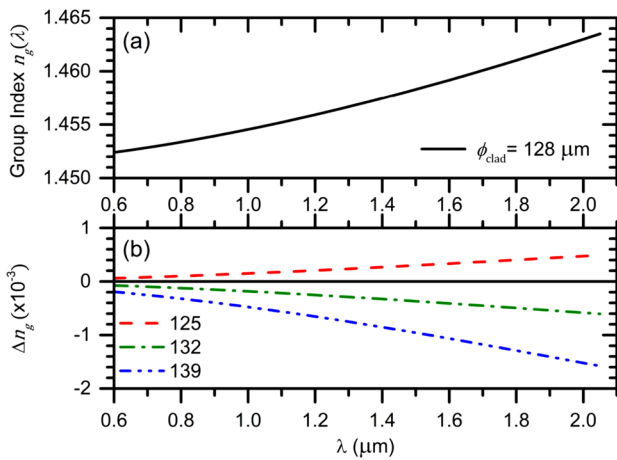


Fig. 3 (a, top) Wavelength dependence of the group index n_g for the PCF with $128 \mu\text{m}$ outer diameter. (b, bottom) Group index difference Δn_g between PCF with outer diameters of 125, 132 and 139 μm and the PCF with $128 \mu\text{m}$ outer diameter taken as reference

the quasi-monochromatic frequency of the chirped signal have a typical duration of $\sqrt{\varphi''}$ of few picoseconds (φ'' is the group delay dispersion introduced on the signal before its amplification). The pulse coherent length L_p is typically of 5 to 10 cm (L_p is due to temporal walk-off resulting from GVM and shall not to be confused with the wave coherent length L_w due to phase mismatch). This further highlights the necessity of using a taper for broadband chirped pulse amplification. Indeed each signal component will only be amplified in a given portion of length L_p within the taper of length L . Consequently, adjusting the pump and signal chirp and delay along with a suitable taper variation rate allows more frequency component to be amplified in a suitable taper portion than in an untapered fiber. The full discussion of f-OPCPA design (taper parameters, chirps rates, pump pulse shaping,...) is still subject to investigation and is not further detailed here as it lies beyond the scope of the present paper.

Figure 4 shows the numerical results from solving the GNLSE for each piece of fiber considered separately (Fig. 4a–d) and for the whole concatenated structure (Fig. 4e). The input pulse considered in the model is characterized by a central wavelength of $1.03 \mu\text{m}$, a peak power of 44 kW and a 50 ps full width at half maximum (FWHM) with a repetition rate of 10 MHz. The effective indices and effective areas of each fiber segments are calculated through the Saitoh and Koshiba empirical method [18]. We can see from Fig. 4a–d that the central wavelengths of the generated idler are slightly red-shifted with the increase of the external fiber diameter. This shift is directly linked to the increase of the local ZDW of the taper as the core diameter increases. The composite idler spectrum of the ensemble (F_0 -to- F_3) is represented on Fig. 4 e. The generated idler spans across the whole bandwidth resulting from the addition of the individual spectra. The use of the taper thus widens the idler spectrum in a considerable manner.

4 Experimental setup

In order to experimentally validate the numerical results, HNL-PCFs have been fabricated, with their characteristics reference in Table 1. In this paper we only report the experimental study of the B taper (and its reverse B'), with a linearly varying external diameter from 125 to 132 μm over a 2 m long piece of fiber. In order to compare it with an untapered fiber, a same HNL-PCF with a constant external diameter of $128 \mu\text{m}$ close to the average B taper diameter has also been fabricated (fiber A).

The pump source developed to characterize the fibers is schematized in Fig. 5. The tunability is obtained by pumping an Ytterbium-doped fiber, which generates an Amplified Spontaneous Emission (ASE) over the 1020 to 1070 nm Ytterbium emission bandwidth. A tunable band-pass spectral filter (Waveshaper 1000A, Finisar) reduces the spectrum to a 0.2 nm bandwidth. After an amplification stage which compensates

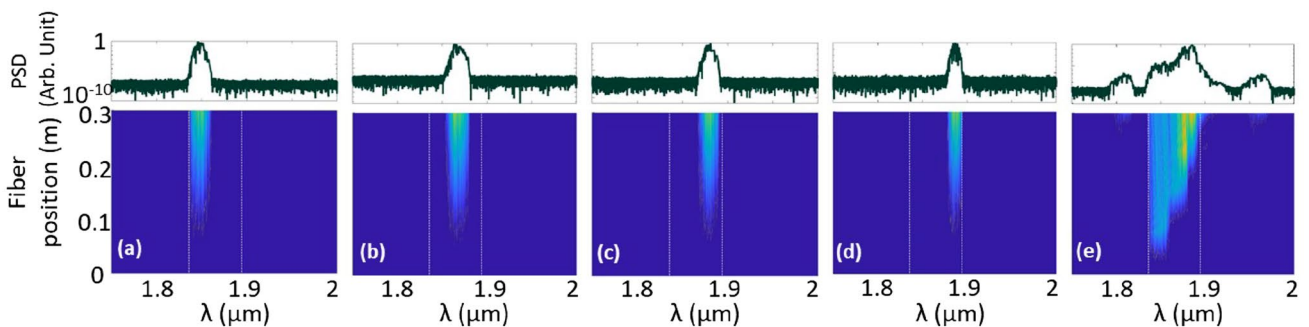


Fig. 4 Numerical simulations of the generated idler spectra along the taper depicted in Fig. 2. The build-up of each spectra for the individual sections (a) F_0 , (b) F_1 , (c) F_2 and (d) F_3 . The build-up of the full taper spectrum (e). The insets correspond to the output generated idler spectra

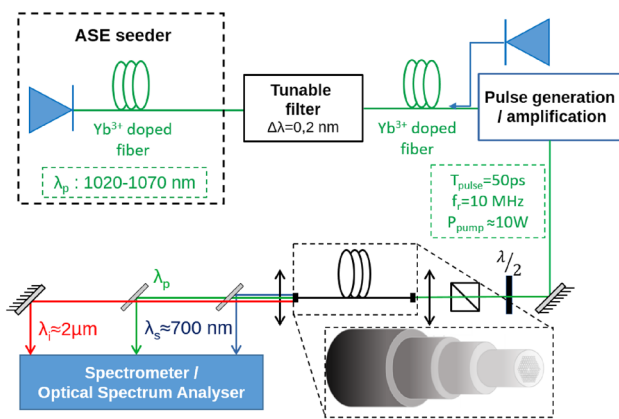


Fig. 5 Experimental setup of the tunable stochastic pump source which allows a characterisation of the tapered fiber

losses induced by the filter, the light seeded a commercial amplification stage (Manny, Irisiome), which not only amplifies the seed wave but also cuts the temporal profile in pulses with a periodicity controlled by an external RF synthesizer. It results in 50 ps pulses train with a repetition rate of 10 MHz, and for a maximum energy of 1 μJ , which corresponds to a peak power of 20 kW, and an average power of 10 W. A telescope is used to adapt the beam size to the numerical aperture of the tapers and a half-wave plate combined with a polarizing cube control the pump power.

Compared with a coherent pumping, an ASE source exhibits numerous advantages for measuring the phasematching curves and/or the gain bandwidth of a nonlinear medium. First, for the same average power, incoherent sources are known to provide an enhanced yield for nonlinear effect [19], making the measurement easier and less likely to damage the material under test. Secondly, parametric gain response are broader with incoherent rather than coherent pumping [20].

The HNL-PCF under test is put on a three-axis support (Nanomax, Thorlabs) and the launched pump beam is done using a 8 mm focal lens. At the fiber output, to separate the pump from the generated idler and signal waves, different dichroic mirrors are used before the analyse of their average spectra with a spectrometer (NIRQuest, Ocean Optics) or an Optical Spectrum Analyser (OSA, AQ6370, Yokogawa). In order to effectively compare the spectrum obtained using either a tapered or an untapered fiber, the experimental study has been done using a pump power which generate 100 mW of signal power, and the same fiber lengths (two meters).

5 Discussion and conclusion

The resulting spectra are reported on Fig. 6 for different pump wavelengths. The idler spectra are a simple conversion of the signal spectra through energy conservation. This

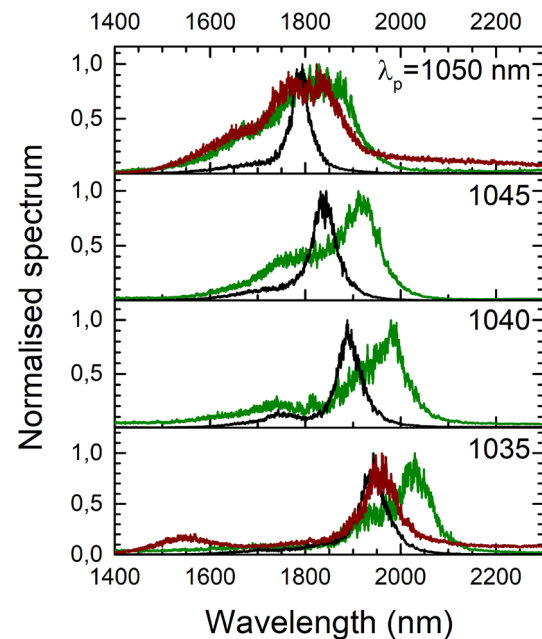


Fig. 6 Experimental idler spectra as a function of the pump wavelength for a d-FWM in the B taper (red), the B' taper (green) and the reference A fiber (black)

conversion has been validated with a mid-IR spectrometer. For sake of comparison, we first recorded the results for an untapered fiber. The reference fiber A idler spectra exhibit a blue detuning with the increase of the pump wavelength, while keeping approximately the same bandwidth: this is the expected behavior for a d-FWM with a pump wave far from the zero-dispersion wavelength [15].

As the reference, all tapers exhibit the same blue detuning as the pump is tuned toward long wavelengths. However, taper generally exhibit a more complex spectrum that peak at a slightly lower frequency than the untapered case. This shift has also been observed in simulation (Fig. 4e).

In order to explain the observed shift towards lower frequencies as compared to fiber A, we discuss below the case of the taper B, and consider the d-FWM parametric generation depending on the taper orientation denoted B as the pump propagates from the small to the large end, and B' as pump propagates from large to small.

One should first recall that for a given pump wavelength, a larger core (i.e. outer diameter here) results in dispersion parameters (ZDW, $\beta_{n,ZD}$) that will generate longer idler wavelength (see Eq. 3). For taper B, shorter idler wavelength are generated first at the small diameter end, and experience the full taper length propagation and gain, while the longer wavelength are only generated at the exit of the large diameter end. Fiber A having a core diameter which is the average of the taper B two end diameters, one might expect the taper B idler spectrum distortion to

be at shorter wavelengths compared to fiber A spectra. Conversely, one expects an idler spectrum distortion toward longer wavelength for taper B' (long wavelength are first generated in the large end and further amplified).

However, we can see that (i) the amount of shift with respect to reference fibre spectra is more or less prominent, and (ii) the spectra are consistently shifted at a longer wavelength than the reference fiber.

While the former effect remains unclear, the latter counter-intuitive effect results from a complex interplay between the variation of the effective nonlinear coefficient γ that depends on the effective mode area A_{eff} (Eq. 2), the varying position at which phasematching (where a substantial parametric gain) occurs for a given idler frequency component, and the accessible build-up length for each component. Among these factors, the most important one is due to the nonlinear dephasing β_{NL} whose increasing values tend to "redshift" the idler branch of the phasematching curve (Eq. 3). Since the taper B contains a whole section (half of the taper length) where the diameter is smaller, the reduced effective mode area results in higher β_{NL} than in fiber A thus resulting in the observed redshift regardless the taper orientation (B or B').

In all cases, the obtained spectra are always broadened compared to a untapered fiber, with for example the 1050 nm pump wavelength, a broadening by a factor of four.

In conclusion, we have presented a new HNL-PCF, with a linearly varying diameter along its length in order to widen its spectral bandwidth. We demonstrated through experiences and simulations a nearly four-times broadening of the spectrum (196 nm corresponds to 24.5 fs coherence time). This indicates that tapers are potentially favorable for the amplification of broadband pulses such as few cycles (4.1 cycles at 1.8 μm) mid-IR pulse in a coherently seeded f-OPCPA configuration and with a suitable recompression. This new technique represents an interesting concept in order to design fibered and broadband mid-IR laser sources since the concept can be extended to any pumping wavelength and fiber structures or materials. Further numerical simulations are needed to understand the potential of this technology and its optimal design parameters.

Author Contributions All XLIM authors contributed to the fiber and tapers elaboration and fabrication. SEA, and SF performed the simulations. GW, JL, and JCD designed the experiment. SEA, GW, and JCD performed the experiment. SEA, RJ, PR, GW, CV, and JCD wrote the main manuscript text. SEA, JCD and GW prepared all figures. All authors reviewed the manuscript.

Funding The authors acknowledge funding by Agence Nationale de la Recherche (ANR) through the project Metropolis (ANR-19-CE47-0008).

Data availability The datasets generated during and/or analysed during the current study are available from the corresponding author on reasonable request.

Declarations

Conflict of interest The authors have no competing interests to declare that are relevant to the content of this article.

Open Access This article is licensed under a Creative Commons Attribution 4.0 International License, which permits use, sharing, adaptation, distribution and reproduction in any medium or format, as long as you give appropriate credit to the original author(s) and the source, provide a link to the Creative Commons licence, and indicate if changes were made. The images or other third party material in this article are included in the article's Creative Commons licence, unless indicated otherwise in a credit line to the material. If material is not included in the article's Creative Commons licence and your intended use is not permitted by statutory regulation or exceeds the permitted use, you will need to obtain permission directly from the copyright holder. To view a copy of this licence, visit <http://creativecommons.org/licenses/by/4.0/>.

References

1. A. Hemming, N. Simakov, J. Haub, A. Carter, A review of recent progress in holmium-doped silica fibre sources. *Opt. Fiber Technol.* **20**(6), 621–630 (2014). <https://doi.org/10.1016/j.yofte.2014.08.010>
2. A. Godard, Infrared (2–12 μm) solid-state laser sources: a review. *Comptes Rendus Physique* **8**(10), 1100–1128 (2007). <https://doi.org/10.1016/j.crhy.2007.09.010>
3. H. Pires, M. Baudisch, D. Sanchez, M. Hemmer, J. Biegert, Ultra-short pulse generation in the mid-ir. *Progress Quantum Electron.* **43**, 1–30 (2015). <https://doi.org/10.1016/j.pquantelec.2015.07.001>
4. J. Rothhardt, S. Hädrich, J.C. Delagnes, E. Cormier, J. Limpert, High average power near-infrared few-cycle lasers. *Laser Photonics Rev.* **11**(4), 1700043 (2017). <https://doi.org/10.1002/lpor.201700043>
5. M. Charbonneau-Lefort, B. Afeyan, M.M. Fejer, Optical parametric amplifiers using chirped quasi-phase-matching gratings i: practical design formulas. *J. Opt. Soc. Am. B* **25**(4), 463–480 (2008). <https://doi.org/10.1364/JOSAB.25.000463>
6. G.M. Archipovaite, S. Petit, J.C. Delagnes, E. Cormier, Yb-fiber laser pumped optical parametric amplifier for probing solid-state systems in the strong field regime. *Opt. Lett.* **42**(5), 891–894 (2017). <https://doi.org/10.1364/OL.42.000891>
7. W. Fu, F.W. Wise, Normal-dispersion fiber optical parametric chirped-pulse amplification. *Opt. Lett.* **43**(21), 5331–5334 (2018)
8. O. Zurita-Miranda, C. Fourcade-Dutin, F. Fauquet, F. Darracq, J.-P. Guillet, P. Mounaix, H. Maillotte, D. Bigourd, Tunable ultrafast infrared generation in a gas-filled hollow-core capillary by a four-wave mixing process. *J. Opt. Soc. Am. B* **39**(3), 662–670 (2022). <https://doi.org/10.1364/JOSAB.444574>
9. C. Caucheteur, D. Bigourd, E. Hugonnot, P. Szriftgiser, A. Kudlinski, M. Gonzalez-Herraez, A. Mussot, Experimental demonstration of optical parametric chirped pulse amplification in optical fiber. *Opt. Lett.* **35**(11), 1786–1788 (2010). <https://doi.org/10.1364/OL.35.001786>
10. T. Godin, Y. Combes, R. Ahmad, M. Rochette, T. Sylvestre, J.M. Dudley, Far-detuned mid-infrared frequency conversion via normal dispersion modulation instability in chalcogenide microwires. *Opt. Lett.* **39**(7), 1885–1888 (2014). <https://doi.org/10.1364/OL.39.001885>

11. D. Nodop, C. Jauregui, D. Schimpf, J. Limpert, A. Tünnermann, Efficient high-power generation of visible and mid-infrared light by degenerate four-wave-mixing in a large-mode-area photonic-crystal fiber. *Opt. Lett.* **34**(22), 3499–3501 (2009). <https://doi.org/10.1364/OL.34.003499>
12. L. Lavoute, J.C. Knight, P. Dupriez, W.J. Wadsworth, High power red and near-ir generation using four wave mixing in all integrated fibre laser systems. *Opt. Express* **18**(15), 16193–16205 (2010). <https://doi.org/10.1364/OE.18.016193>
13. C. Jauregui, A. Steinmetz, J. Limpert, A. Tünnermann, High-power efficient generation of visible and mid-infrared radiation exploiting four-wave-mixing in optical fibers. *Opt. Express* **20**(22), 24957–24965 (2012). <https://doi.org/10.1364/OE.20.024957>
14. T. Gottschall, T. Meyer, M. Schmitt, J. Popp, J. Limpert, A. Tünnermann, Four-wave-mixing-based optical parametric oscillator delivering energetic, tunable, chirped femtosecond pulses for non-linear biomedical applications. *Opt. Express* **23**(18), 23968–23977 (2015). <https://doi.org/10.1364/OE.23.023968>
15. J.C. Delagnes, R. Royon, J. Lhermite, G. Santarelli, noz, H.M., Grosz, T., Darwich, D., Dauliat, R., Jamier, R., Roy, P., Cormier, E., High-power widely tunable ps source in the visible light based on four wave mixing in optimized photonic crystal fibers. *Opt. Express* **26**(9), 11265–11275 (2018). <https://doi.org/10.1364/OE.26.011265>
16. G. Walter, D. Descloux, J.-B. Dherbecourt, J.-M. Melkonian, M. Raybaut, C. Drag, A. Godard, Picosecond synchronously pumped optical parametric oscillator based on chirped quasi-phase matching. *J. Opt. Soc. Am. B* **37**(2), 552–563 (2020). <https://doi.org/10.1364/JOSAB.380605>
17. J.M. Dudley, G. Genty, S. Coen, Supercontinuum generation in photonic crystal fiber. *Rev. Mod. Phys.* **78**, 1135–1184 (2006). <https://doi.org/10.1103/RevModPhys.78.1135>
18. K. Saitoh, M. Koshiba, Empirical relations for simple design of photonic crystal fibers. *Opt. Express* **13**(1), 267–274 (2005). <https://doi.org/10.1364/OPEX.13.000267>
19. N. Valero, D. Marion, J. Lhermite, J.-C. Delagnes, W. Renard, R. Royon, E. Cormier, High-power amplified spontaneous emission pulses with tunable coherence for efficient non-linear processes. *Sci. Rep.* **1**(11), 4844 (2021). <https://doi.org/10.1038/s41598-021-83443-2>
20. A. Sauter, S. Pitois, G. Millot, A. Picozzi, Incoherent modulation instability in instantaneous nonlinear kerr media. *Opt. Lett.* **30**(16), 2143–2145 (2005). <https://doi.org/10.1364/OL.30.002143>

Publisher's Note Springer Nature remains neutral with regard to jurisdictional claims in published maps and institutional affiliations.